

# Entropy production of non-reciprocal interactions

Ziluo Zhang (张子洛)<sup>1</sup> and Rosalba Garcia-Millan<sup>2,3,\*</sup>

<sup>1</sup>Department of Mathematics, Imperial College London, London SW7 2AZ, UK

<sup>2</sup>DAMTP, Centre for Mathematical Sciences, University of Cambridge, Cambridge CB3 0WA, UK

<sup>3</sup>St John's College, University of Cambridge, Cambridge CB2 1TP, UK

(Dated: November 28, 2022)

Non-reciprocal interactions are present in many systems out of equilibrium. The rate of entropy production is a measure that quantifies the time irreversibility of a system, and thus how far it is from equilibrium. In this work, we introduce a non-motile active particle system where activity originates from asymmetric, pairwise interaction forces that result in an injection of energy at the microscopic scale. We calculate stationary correlation functions and entropy production rate in three exactly solvable cases, and analyse a more general case in a perturbation theory as an expansion in weak interactions using a fully microscopic description. Our results show that equilibrium may be recovered by adjusting the diffusion constants despite non-reciprocity, revealing an equivalence in the absolute amplitude of the force and diffusivity. We support our analytical results with numerical simulations.

**Introduction.**—Non-reciprocal interactions are those that do not obey Newton's third law (*actio equal reactio*). These generate intrinsically out-of-equilibrium dynamics [1–3] and are often invoked to model striking dynamical pattern formation such as flocking [4, 5], worming [6] or travelling states [7]. Common mechanisms that break reciprocity are (anti-)alignment [8] and vision cone interactions [9–11]. Non-reciprocal interactions between two species play a crucial role in numerous biological processes, such as predator-prey dynamics [12, 13] or collective cell migration [14]. Non-reciprocity is found in attractive-repulsive interactions giving rise, for example, to the chase-and-run dynamics present between a dog and a herd of sheep [14]: while the dog runs toward the sheep, sheep fearfully run away from the dog, following a trajectory such as in Fig. 1(a).

Systems with non-reciprocal interactions are generally out of equilibrium, which is characterised by the breakdown of time-reversal symmetry. The rate of entropy production has become, over the last decade, a prominent measure of irreversibility that quantifies how far from equilibrium a system is [15–18]. Measuring and calculating the entropy production rate is, therefore, key to understanding the non-equilibrium behaviour of a system and poses a major theoretical challenge in the case of interacting many-particle active systems. Recent studies have focused on the thermodynamic properties of non-reciprocity in a system described by coupled, linear Langevin equations [1, 2, 19]. Reference [1] showed that there exist systems with non-reciprocal interactions that do satisfy detailed balance. However, a fully microscopic calculation of the entropy production of a many-particle system with non-linear and non-reciprocal interaction forces is lacking. The power of microscopic theories in the study of active particle systems lies in the direct link they establish between agents' properties and their emergent phenomena. Deriving exact results that serve as benchmark is thus of paramount importance [15, 17].

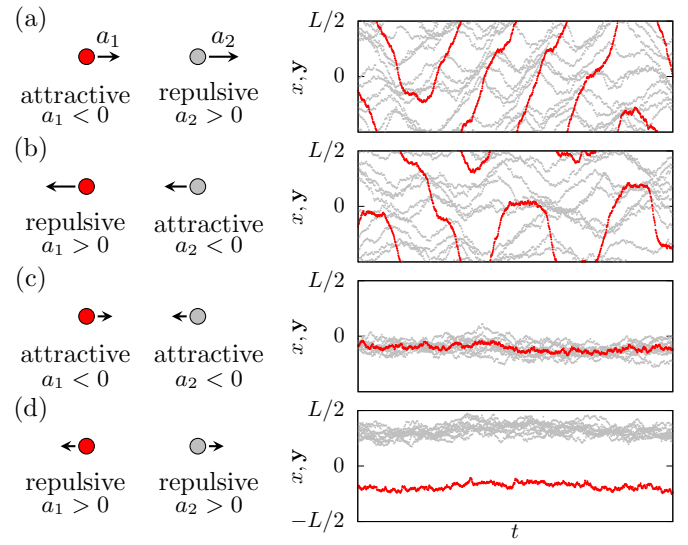


FIG. 1. **Particle trajectories** ( $x, y$ ) described by Eq. (1) with one particle of species A (red) and  $N = 10$  particles of species B (grey), sinusoidal interacting potentials, equal diffusivities and zero drifts. The sign of potential amplitudes  $a_1$  and  $a_2$  are indicated on the left. Interactions are non-reciprocal in (a) and (b) and reciprocal in (c) and (d). In this example, since  $D_1 = D_2$ , non-reciprocal systems are active and reciprocal systems are passive.

In this letter, we introduce a non-motile active particle system that is driven out of equilibrium by non-reciprocal interactions between one particle and the rest [20]. We use a fully microscopic description to calculate correlation functions and entropy production. We consider three exactly solvable cases and a fourth, more general case using a perturbative field theory. Our perturbative approach provides a systematic framework to calculate correlation functions and the short-time propagator, both of which are essential to calculate the entropy production rate [15, 21–23]. Our analytical results are

compared with the average rate of dissipated heat along the stochastic trajectories of the particles in Sekimoto's framework [1, 24–26], showing good agreement within the domain where our perturbative treatment holds. We address the regime of small to intermediate particle numbers, and establish the path from microscopic dynamics to emergent effective interactions.

Following the example of chase-and-run dynamics described above, we consider a one-dimensional system with two types of particles: one particle of species A at position  $x$  and  $N$  particles of species B at  $\mathbf{y} = (y_1, \dots, y_N)$ , with diffusion constants  $D_1$  and  $D_2$ , and drifts  $u_1$  and  $u_2$ , that live on a ring of length  $L$ . The interaction forces are mediated by the periodic and bounded pair potentials  $V_1$  and  $V_2$ , resulting in the additional effective drifts  $-\sum_i \partial_x V_1(x - y_i)$  for particle A and  $-\partial_{y_i} V_2(y_i - x)$  for each particle B. According to the structure of these pair interactions, B particles do not directly interact with each other, although their trajectories are effectively coupled by means of particle A, as we discuss below.

The system dynamics are described by the coupled, overdamped Langevin equations,

$$\dot{x} = u_1 - \sum_{i=1}^N V'_1(x - y_i) + \xi(t) , \quad (1a)$$

$$\dot{y}_i = u_2 - V'_2(y_i - x) + \xi_i(t) , \quad (1b)$$

where  $\xi$  and  $\xi_i$  are Gaussian white noises, with correlators  $\langle \xi(t)\xi(t') \rangle = 2D_1\delta(t - t')$  and  $\langle \xi_i(t)\xi_j(t') \rangle = 2D_2\delta_{i,j}\delta(t - t')$ . We assume Boltzmann constant and mobility to be unity, and therefore deem the diffusion constants to essentially be temperatures. The stationary probability currents of  $x$  and  $y_i$  are  $J_x = -\left(-u_1 + \sum_{i=1}^N V'_1(x - y_i) + D_1\partial_x\right)P(x, \mathbf{y})$  and  $J_{y_i} = -\left(-u_2 + V'_2(y_i - x) + D_2\partial_{y_i}\right)P(x, \mathbf{y})$ , where  $P(x, \mathbf{y})$  is the joint probability density of state  $x, \mathbf{y}$  [27]. If inter-

actions are reciprocal, namely the interaction potentials satisfy  $V_1(\ell) = V_2(\ell) \equiv V(\ell)$  with  $\ell = x - y$ , then forces are conservative because Eq. (1) can be derived from the Hamiltonian  $\mathcal{H} = -u_1x + \sum_{i=1}^N (-u_2y_i + V(x - y_i))$ . Conversely, non-reciprocal interactions result in non-conservative forces. Fig. 1 shows particle trajectories described by Eq. (1) with different combinations of attractive and repulsive potentials, illustrating the breakdown of time-reversal symmetry in the active systems in Figs. 1(a) and 1(b), in contrast to the passive systems in Figs. 1(c) and 1(d). We simulate particle trajectories described by Eq. (1) using standard Brownian dynamics simulations.

We calculate the entropy production to quantify the irreversibility of this system [16–18]. In Gaspard's framework [16], the entropy production of a Markov process is

$$\dot{S}(t) = \lim_{\tau \rightarrow 0} \frac{1}{(N!)^2} \int_0^L dx dx' d^N y d^N y' \left\{ P(x, \mathbf{y}; t) \dot{W}(x, \mathbf{y} \rightarrow x', \mathbf{y}'; \tau) \right. \\ \left. \times \ln \left( \frac{P(x, \mathbf{y}; t) W(x, \mathbf{y} \rightarrow x', \mathbf{y}'; \tau)}{P(x', \mathbf{y}'; t) W(x', \mathbf{y}' \rightarrow x, \mathbf{y}; \tau)} \right) \right\} , \quad (2)$$

where  $W(x, \mathbf{y} \rightarrow x', \mathbf{y}'; \tau)$  is the transition probability for the system to go from state  $x, \mathbf{y}$  to state  $x', \mathbf{y}'$  in an interval of time  $\tau$ . The Gibbs factor  $1/N!$  in each integral over  $\mathbf{y}$  in Eq. (2) accounts for the phase space of the positions of B particles being that of indistinguishable particles in the continuum, where the probability that two particles are found at the same position has zero measure.

Using the framework established in [15], the entropy production in Eq. (2) in the stationary state simplifies to

$$\dot{S} = \int_0^L dx dy \left\{ -V''_1(x - y) + \frac{1}{D_1} \left( \frac{u_1}{N} - V'_1(x - y) \right)^2 - V''_2(y - x) + \frac{1}{D_2} (u_2 - V'_2(y - x))^2 \right\} P_2^{(1+N)}(x, y) \\ + \int_0^L dx dy dy' \frac{1}{D_1} \left( \frac{u_1}{N} - V'_1(x - y) \right) \left( \frac{u_1}{N} - V'_1(x - y') \right) P_3^{(1+N)}(x, y, y') , \quad (3)$$

which is derived in the Supplemental Material (SM). Eq. (3) shows that the entropy production of this system depends on the two-point  $P_2^{(1+N)}$  and three-point  $P_3^{(1+N)}$  correlation functions [15]. In the absence of an exact solution, we calculate these correlation functions perturbatively, using a Doi-Peliti field theory that captures the microscopic dynamics of Eq. (1).

*Two-particle system.*—The system with one particle of

each species is tractable exactly. Without self-propulsion,  $u_1 = u_2 = 0$ , the two-point correlation function is the barometric formula [27, 28]

$$P_2^{(2)}(x, y) = \frac{1}{L\mathcal{N}} e^{-\frac{V_1(x-y)+V_2(y-x)}{D_1+D_2}} , \quad (4)$$

with  $\mathcal{N}$  such that  $\int_0^L dx dy P_2^{(2)}(x, y) = 1$ , which is represented with dashed lines in Fig. 2. The three-point

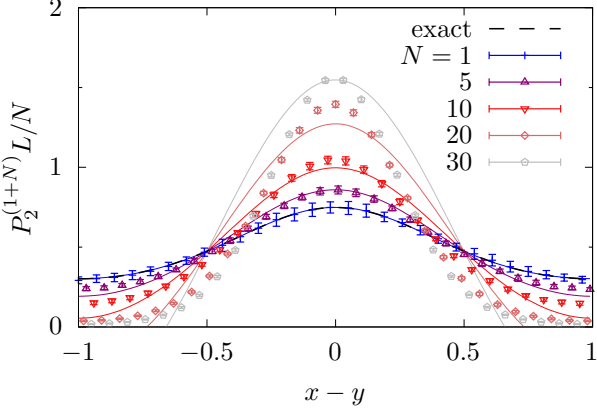


FIG. 2. **Rescaled two-point correlation function**  $P_2^{(1+N)}(x, y)$  of A and B particles at  $x$  and  $y$ , with sinusoidal interaction potentials and  $a_1 = -0.2$ ,  $a_2 = -0.3$ ,  $u_1 = u_2 = 0$ ,  $D_1 = 1$ ,  $D_2 = 0.1$ ,  $L = 2$ . Symbols show numerical estimates; dashed lines, exact result Eq. (4); and solid lines, perturbative prediction (SM).

correlation function is naturally  $P_3^{(2)} = 0$ . Setting the probability currents to zero,  $J_x = 0$  and  $J_y = 0$ , gives the condition for detailed balance for this system,

$$\frac{V'_1(x-y)}{D_1} = -\frac{V'_2(y-x)}{D_2}, \quad (5)$$

showing an equivalent role in the amplitude of interaction force and diffusion. *The system can therefore be out of equilibrium due to particle interactions even in the absence of self-propulsion.* The detailed balance condition in Eq. (5) is consistent with the detailed balance condition found in [1] for the special case of harmonic interaction potentials. Using Eq. (4) in Eq. (3), the stationary entropy production is

$$\dot{S} = \int_0^L d\ell \frac{\rho(\ell)}{D_1 + D_2} \left( \sqrt{\frac{D_2}{D_1}} V'_1(\ell) + \sqrt{\frac{D_1}{D_2}} V'_2(-\ell) \right)^2, \quad (6)$$

where  $\rho(x-y) = LP_2^{(2)}(x, y)$ . The entropy production is zero only if Eq. (5) is satisfied. Fig. 3 shows  $\dot{S}$  for the two-particle case,  $N = 1$ , for sinusoidal interaction potentials,

*Equilibrium system.*—Imposing the detailed balance condition in Eq. (5) and zero drifts  $u_1 = u_2 = 0$ , the stationary joint probability density is

$$P(x, y) = \frac{1}{L\mathcal{N}} e^{-\sum_{i=1}^N \frac{V_1(x-y_i) + V_2(y_i-x)}{D_1 + D_2}}, \quad (7)$$

with normalisation  $\mathcal{N}$  such that  $\int_0^L dx d^N y P(x, y) = N!$ . The probability currents vanish, implying that the detailed balance condition in Eq. (5) generalises to the many-particle system.

*Chase and run.*—The limiting case where interaction forces between species are attractive-repulsive with equal

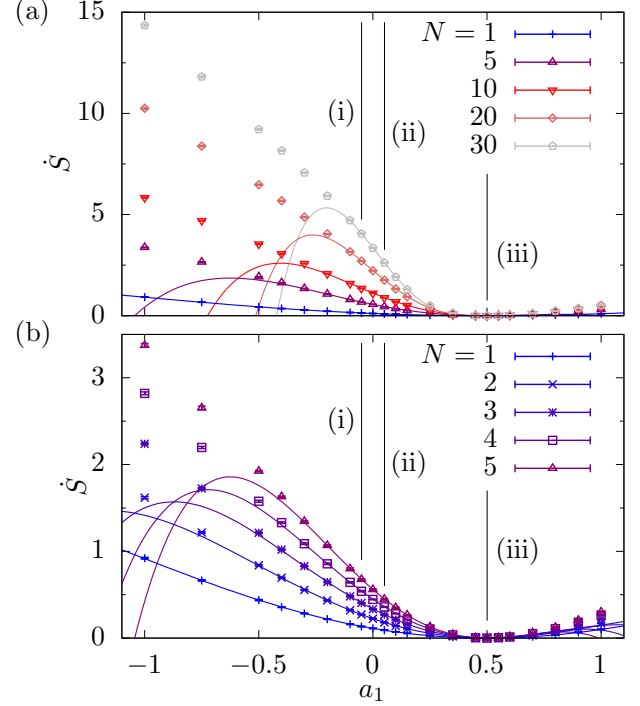


FIG. 3. **Entropy production**  $\dot{S}$  varying  $a_1$ , (a)  $N \in \{1, \dots, 30\}$  and (b)  $N \in \{1, \dots, 5\}$ , and fixed  $a_2 = 0.05$ ,  $D_1 = 1$ ,  $D_2 = 0.1$ ,  $u_1 = u_2 = 0$ ,  $L = 2$ . Symbols indicate numerical estimates using Sekimoto's framework, and lines perturbative prediction in (SM). The cases (i) chase-and-run dynamics  $a_1 = -a_2$ , (ii) reciprocal interactions  $a_1 = a_2$ , and (iii) equilibrium  $a_1 = a_2 D_1 / D_2$ , are indicated. The system with reciprocal interactions is out of equilibrium because  $D_1 \neq D_2$ , Eq. (5).

magnitude and equal directions is of particular interest both for its biological motivation [14], as well as for its mathematical tractability. Assuming that interaction potentials satisfy  $V_1(\ell) = -V_2(-\ell) \equiv V(\ell)$ , the two-particle system is uniformly distributed, Eq. (4), because the distance  $\ell = x - y$  diffuses in the comoving frame, and it is the centre of mass that spins with velocity  $-V'(\ell)$ . By the same reasoning, the stationary joint probability density stays uniform when adding new particles to the system. By marginalisation, the  $n$ -point correlation function is

$$P_n^{(1+N)}(x, y_1, \dots, y_{n-1}) = \frac{N!}{(N-n+1)!L^n}, \quad (8)$$

for  $n \geq 1$ . The entropy production in Eq. (3) is, thus,

$$\dot{S} = \frac{N}{L} \left( \frac{1}{D_1} + \frac{1}{D_2} \right) \int_0^L d\ell (V'(\ell))^2, \quad (9)$$

yielding an exact result for arbitrary particle number  $N$ . Eq. (9) shows that the system with attractive-repulsive interactions is out of equilibrium independently of the

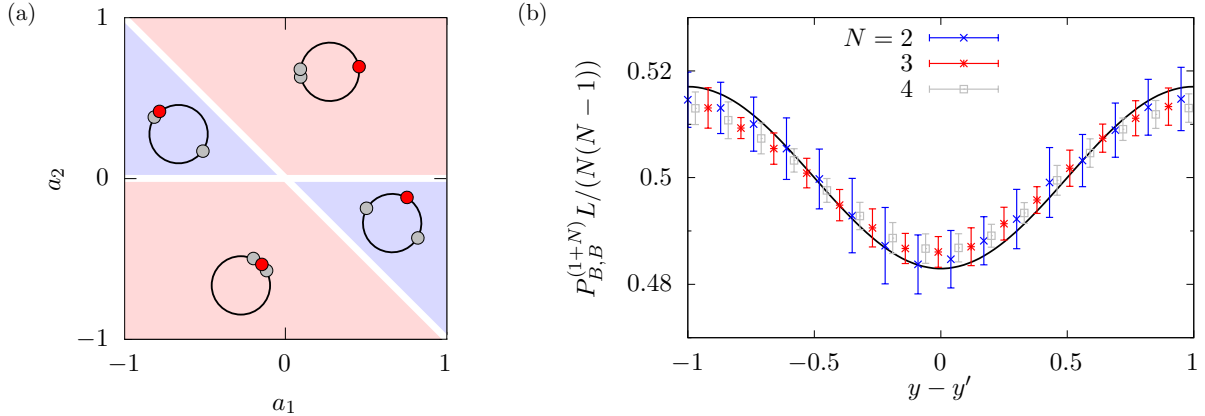


FIG. 4. **Effective interactions** between particles of species B. (a) Phase diagram showing effective attraction (red) and repulsion (blue) varying  $a_1$  and  $a_2$ , as predicted by the amplitude of the two-point correlation function  $P_{B,B}^{(1+N)}(y, y')$  of two B particles at  $y$  and  $y'$ , in the presence of an A particle, insets show frequent configurations in each regime. (b) Rescaled  $P_{B,B}^{(1+N)}$ , with sinusoidal interaction potentials, and  $a_1 = -0.2$ ,  $a_2 = 0.15$ ,  $D_1 = 1$ ,  $D_2 = 0.1$ ,  $u_1 = u_2 = 0$ ,  $L = 2$ . Symbols indicate numerical estimates, and solid line, perturbative result (SM).

magnitude of interaction forces, as indicated in Fig. 3. Indeed, the *chaser* tends to run behind the *chased*, exhibiting the breakdown of time-reversal symmetry.

*Sinusoidal interaction potentials.*—To explore the parameter space of attractive and repulsive interactions, we consider sinusoidal potentials  $V_1(\ell) = a_1 \cos k_1 \ell$  and  $V_2(\ell) = a_2 \cos k_1 \ell$ , with  $k_1 = 2\pi/L$ . The signs of  $a_1$  and  $a_2$  determine whether interactions are attractive or repulsive: negative amplitudes result in attraction, whereas positive amplitudes result in repulsion, as shown in Fig. 1.

We derive the two-point and three-point correlation functions, in a perturbative expansion valid at small amplitudes  $a_1$  and  $a_2$  compared to the diffusion constants  $D_1$  and  $D_2$  in the SM. In Fig. 2, we show the two-point correlation function  $P_2^{(1+N)}(x, y)$  of the A particle at position  $x$  and one out of  $N$  particles of species B at  $y$ , as a function of the distance  $x - y$ , varying  $N$ . Due to attractive interactions, short distances are favoured over longer distances, which is more prominent as  $N$  increases. Fig. 2 shows good agreement for small to intermediate  $N$  and illustrates how the deviation of the numerical estimates from the perturbative prediction increases with  $N$ .

Using the correlation functions  $P_2^{(1+N)}$  and  $P_3^{(1+N)}$  in Eq. (3) we obtain the entropy production  $\dot{S}$ , derived in the SM, which is shown in Fig. 3 as a function of  $a_1$  (solid lines). The behaviour of  $\dot{S}$  is shown for two ranges of  $N$ : the small to large particle number in Fig. 3(a), and the small to intermediate particle numbers in Fig. 3(b). Following Sekimoto's framework [1, 24–26], in Fig. 3 we compare the perturbative result for  $\dot{S}$  with the total entropy production  $\dot{S} = \dot{Q}_x/\mathcal{T}_1 + \sum_{i=1}^N \dot{Q}_{y_i}/\mathcal{T}_2$  estimated numerically from the average rate of dissipated energy along particle trajectories,  $\dot{Q}_x = \langle (\dot{x}(t) - \xi(t)) \circ d\mathbf{x}(t) \rangle / dt$  and

$\dot{Q}_{y_i} = \langle (y_i(t) - \xi_i(t)) \circ dy_i(t) \rangle / dt$ , where  $\circ$  denotes the Stratonovich product and where the temperatures are  $\mathcal{T}_1 = D_1/(k_B\mu)$ , and  $\mathcal{T}_2 = D_2/(k_B\mu)$ , with Boltzmann constant  $k_B$  and mobility  $\mu$  set to unity.

Fig. 3 shows that the entropy production  $\dot{S}$  increases smoothly for amplitudes away from the equilibrium  $a_1 = a_2 D_1/D_2$ , and for increasing  $N$ . It further shows that  $\dot{S}$  grows faster in the attractive-repulsive regime ( $a_1 < 0$ ) than in the repulsive-repulsive regime ( $a_1 > 0$ ). The cases of chase-and-run dynamics, reciprocal interactions and equilibrium are indicated. Here, since the diffusion constants are different,  $D_1 \neq D_2$ , the system with reciprocal interactions does not satisfy the condition for detailed balance in Eq. (5) and is thus out of equilibrium. The agreement is excellent between numerical results and perturbative predictions within the validity regime, that is for  $|a_1|$  and  $N$  sufficiently small. Increasing either of those parameters leads to larger deviation of the numerical estimates from the perturbative prediction.

*Effective interactions.*—Although particles of species B do not directly interact with each other according to Eq. (1), their trajectories are correlated through the particle of species A, as illustrated in Fig. 1. In Figs. 1(c) and (d), for instance, B particles visibly display effective attraction. Marginalising the three-point correlation function,  $\int_0^L dx P_3^{(1+N)}(x, y, y') = P_{B,B}^{(1+N)}(y, y')$ , reveals correlations between any two particles of species B at positions  $y$  and  $y'$ , that we identify as effective interactions, with a sign (attractive or repulsive) that depends on the amplitudes  $a_1$  and  $a_2$ , derived in the SM. We found that B particles display effective repulsion if  $a_1 > -a_2 > 0$  or  $-a_1 > a_2 > 0$  (blue area in the phase diagram in Fig. 4(a)), no correlation if  $a_1 = -a_2$  or  $a_2 = 0$  (white lines), and effective attraction other-

wise (red area). Based on this prediction, which is of second order in the perturbation expansion, we explored the two-point correlation function  $P_{B,B}^{(1+N)}$  for an example of effective repulsion in the regime  $-a_1 > a_2 > 0$ , see Fig. 4(b), which shows that long distances are more frequent than short distances between any two B particles. The underlying microscopic mechanism is the following: the attraction felt by particle A is stronger than the repulsion felt by B particles, so that A captures one of the B particles, while the rest escape.

*Conclusions.*— We have studied the role of non-reciprocal interactions in the environmental entropy change using a fully microscopic description. We have shown that non-reciprocal forces generally break detailed balance, resulting in a local injection of energy and turning a system of non-motile particles into an active one. To our knowledge, this is the first microscopic field theory of an interacting, many-particle active system. Our framework can be extended to estimate the extractable work in other physical systems, such as asymmetrically shaped objects immersed in active baths that have been proposed in the context of autonomous engines.

We are grateful to G. Pruessner for introducing us to field theory and for seminal discussions about the barometric formula. We also thank S. Loos, C. Scalliet, M. Cates, T. Agranov, P. Pietzonka, G. Biroli, B. Walther, L. Cocconi and Z. Zhen for useful discussions. RG-M was supported in part by the European Research Council under the EU’s Horizon 2020 Programme (Grant number 740269), and acknowledges support from a St John’s College Research Fellowship, University of Cambridge.

---

\* rg646@cam.ac.uk

- [1] S. Loos and S. Klapp. Irreversibility, heat and information flows induced by non-reciprocal interactions. *New J. Phys.*, 22(12):123051, 2020.
- [2] C. Godrèche and J.-M. Luck. Characterising the nonequilibrium stationary states of ornstein-uhlenbeck processes. *J. Phys. A: Math. Theor.*, 52(3):035002, 2018.
- [3] T. Kano, K. Osuka, T. Kawakatsu, and A. Ishiguro. Mathematical analysis for non-reciprocal-interaction-based model of collective behavior. *J. Phys. Soc. Japan*, 86(12):124004, 2017.
- [4] A. Cavagna, I. Giardina, and T. S. Grigera. The physics of flocking: Correlation as a compass from experiments to theory. *Phys. Rep.*, 728:1–62, 2018.
- [5] M. Nagy, Z. Ákos, D. Biro, and T. Vicsek. Hierarchical group dynamics in pigeon flocks. *Nature*, 464(7290):890–893, 2010.
- [6] A. Deblais, A. Maggs, D. Bonn, and S. Woutersen. Phase separation by entanglement of active polymerlike worms. *Phys. Rev. Lett.*, 124:208006, 05 2020.
- [7] Z. You, A. Baskaran, and M. C. Marchetti. Nonreciprocity as a generic route to traveling states. *Proc. Natl. Acad. Sci. USA*, 117(33):19767–19772, 2020.
- [8] M. Fruchart, R. Hanai, P. B. Littlewood, and V. Vitelli. Non-reciprocal phase transitions. *Nature*, 592(7854):363–369, 2021.
- [9] M. Durve, A. Saha, and A. Sayeed. Active particle condensation by nonreciprocal and time-delayed interactions. *Eur. Phys. J. E*, 41:49, 2018.
- [10] L. Barberis and F. Peruani. Large-scale patterns in a minimal cognitive flocking model: Incidental leaders, nematic patterns, and aggregates. *Phys. Rev. Lett.*, 117(24), 2016.
- [11] S. Loos, S. Klapp, and T. Martynec. Long-range order and directional defect propagation in the non-reciprocal xy model with vision cone interactions. *arXiv:2206.10519*, 2022.
- [12] S. Redner and P. L. Krapivsky. Capture of the lamb: Difusing predators seeking a diffusing prey. *Am. J. Phys.*, 67(12):1277–1283, 1999.
- [13] C. Meredith, P. Moerman, J. Groenewold, Y.-J. Chiu, W. Kegel, A. van Blaaderen, and L. Zarzar. Predator-prey interactions between droplets driven by non-reciprocal oil exchange. *Nat. Chem.*, 12(12):1136–1142, 2020.
- [14] B. Stramer and R. Mayor. Mechanisms and in vivo functions of contact inhibition of locomotion. *Nat. Rev. Mol. Cell Biol.*, 18:43–55, 2017.
- [15] G. Pruessner and R. Garcia-Millan. Field theories of active particle systems and their entropy production. *arXiv:2211.11906 [cond-mat.stat-mech]*, 2022.
- [16] P. Gaspard. Time-reversed dynamical entropy and irreversibility in Markovian random processes. *J. Stat. Phys.*, 117(3):599–615, 2004.
- [17] L. Cocconi, R. Garcia-Millan, Z. Zhen, B. Buturca, and G. Pruessner. Entropy production in exactly solvable systems. *Entropy*, 22(11):1252, 2020.
- [18] H. Alston, L. Cocconi, and T. Bertrand. Non-equilibrium thermodynamics of diffusion in fluctuating potentials. *J. Phys. A: Math. Theor.*, 2022.
- [19] M. Brandenbourger, X. Locsin, E. Lerner, and C. Coulais. Non-reciprocal robotic metamaterials. *Nature communications*, 10(1):1–8, 2019.
- [20] Henry Alston, Andrew O Parry, Raphaël Voituriez, and Thibault Bertrand. Intermittent attractive interactions lead to microphase separation in non-motile active matter. *arXiv:2201.04091*, 2022.
- [21] Z. Zhang and G. Pruessner. Field theory of free run and tumble particles in  $d$  dimensions. *J. Phys. A*, 2021.
- [22] R. Garcia-Millan and G. Pruessner. Run-and-tumble motion in a harmonic potential: field theory and entropy production. *J. Stat. Mech.: Theory Exp.*, 2021(6):063203, 2021.
- [23] M. Bothe, L. Cocconi, Z. Zhen, and G. Pruessner. Particle entity in the doi-peliti and response field formalisms. *arXiv:2205.10409*, 2022.
- [24] K. Sekimoto. *Stochastic energetics*, volume 799. Springer, 2010.
- [25] A. Ghosal and G. Bisker. Inferring entropy production rate from partially observed langevin dynamics under coarse-graining. *arXiv:2205.14688*, 2022.
- [26] É. Roldán, J. Barral, P. Martin, J. Parrondo, and F. Jülicher. Quantifying entropy production in active fluctuations of the hair-cell bundle from time irreversibility and uncertainty relations. *New J. Phys.*, 23(8):083013, 2021.
- [27] H. Risken. *The Fokker-Planck Equation: Methods of Solutions and Applications*, 2nd ed. Springer Verlag, Berlin,

Heidelberg, 1989.

[28] L. Feherlei, M. Polackova, Z. Zhang, and G. Pruessner. Field theory of active brownian particles in potentials. To be published, 2022.

[29] U. C. T'über, M. Howard, and B. P. Vollmayr-Lee. Applications of field-theoretic renormalization group methods to reaction-diffusion problems. *J. Phys. A: Math. Gen.*, 38(17):R79–R131, 2005.

[30] J. Cardy. Reaction-diffusion processes. In *Nonequilibrium Statistical Mechanics and Turbulence*, pages 108–161. Cambridge University Press, 2008.

[31] M. Doi. Second quantization representation for classical many-particle system. *J. Phys. A: Math. Gen.*, 9(9):1465–1477, 1976.

[32] Zigan Zhen and Gunnar Pruessner. Optimal ratchet potentials for run-and-tumble particles. *arXiv:2204.04070*, 2022.

## Supplemental Material: Entropy production of non-reciprocal interactions

Ziluo Zhang and Rosalba Garcia-Millan

### ENTROPY PRODUCTION

We calculate the internal entropy production rate in Eq. (2) of this Markov process via [15–18]. At stationarity, the internal entropy production simplifies as the probability  $P$  disappears from the logarithm [15, 17, 22],

$$\dot{S} = \lim_{\tau \rightarrow 0} \frac{1}{(N!)^2} \int_0^L dx dx' d^N y d^N y' P(x, \mathbf{y}) \dot{W}(x, \mathbf{y} \rightarrow x', \mathbf{y}'; \tau) \ln \left( \frac{W(x, \mathbf{y} \rightarrow x', \mathbf{y}'; \tau)}{W(x', \mathbf{y}' \rightarrow x, \mathbf{y}; \tau)} \right) , \quad (\text{S-1})$$

where  $P(x, \mathbf{y}) = \lim_{t \rightarrow \infty} P(x, \mathbf{y}; t)$  is the stationary density. Following the approach in [15] we obtain the transition rate  $\lim_{\tau \rightarrow 0} \dot{W}(x, \mathbf{y} \rightarrow x', \mathbf{y}'; \tau) = \dot{W}(x, \mathbf{y} \rightarrow x', \mathbf{y}'; 0)$  from the Fokker-Planck Eq. (S-7),

$$\dot{W}(x, \mathbf{y} \rightarrow x', \mathbf{y}'; 0) = \left\{ D_1 \partial_{x'}^2 - u_1 \partial_{x'} + \sum_{i=1}^N \left( D_2 \partial_{y_i'}^2 - u_2 \partial_{y_i'} + V_1'(x - y_i) \partial_{x'} + V_2'(y_i - x) \partial_{y_i'} \right) \right\} \delta(x' - x) \delta(\mathbf{y}' - \mathbf{y}) , \quad (\text{S-2})$$

and the short-time limit of the logarithm of the ratio of propagators,

$$\lim_{\tau \rightarrow 0} \ln \left( \frac{W(x, \mathbf{y} \rightarrow x', \mathbf{y}'; \tau)}{W(x', \mathbf{y}' \rightarrow x, \mathbf{y}; \tau)} \right) = \sum_{i=1}^N \left\{ \frac{x' - x}{2D_1} \left( \frac{u_1}{N} - V_1'(x - y_i) + \frac{u_1}{N} - V_1'(x' - y_i') \right) \right. \\ \left. + \frac{y_i' - y_i}{2D_2} (u_2 - V_2'(y_i - x) + u_2 - V_2'(y_i' - x')) \right\} . \quad (\text{S-3})$$

Substituting Eqs. (S-2) and (S-3) into (S-1), using the normalisation that accounts for B particles being indistinguishable  $\int_0^L dx d^N y P(x, \mathbf{y}) = N!$ , and integrating by parts, we obtain

$$\dot{S} = \frac{1}{N!} \int_0^L dx d^N y \left\{ - \sum_{i=1}^N V_1''(x - y_i) + \frac{1}{D_1} \left( u_1 - \sum_{i=1}^N V_1'(x - y_i) \right)^2 \right. \\ \left. - \sum_{i=1}^N V_2''(y_i - x) + \sum_{i=1}^N \frac{1}{D_2} (u_2 - V_2'(y_i - x))^2 \right\} P(x, \mathbf{y}) . \quad (\text{S-4})$$

Using the following marginalisation property of the  $n$ -point correlation function,

$$\int dy_{n-1} P_n^{(1+N)}(x, y_1, \dots, y_{n-1}) = (N - n + 2) P_{n-1}^{(1+N)}(x, y_1, \dots, y_{n-2}) , \quad (\text{S-5})$$

we arrive at Eq. (3).

In the many-particle system with sinusoidal interaction potentials and zero drift, the leading order behaviour of the entropy production is obtained by substituting Eqs. (S-28) and (S-32) into Eq. (3),

$$\dot{S} = \frac{2\pi^2 N}{L^2} \left[ \left( \frac{a_1^2}{D_1} + \frac{a_2^2}{D_2} - \frac{(a_1 + a_2)^2}{D_1 + D_2} \right) \left( 1 - \frac{1}{8} \left( \frac{a_1 + a_2}{D_1 + D_2} \right)^2 \right) - (N - 1) \frac{a_1(a_1 + a_2)(D_1 a_2 - D_2 a_1)^2}{D_1 D_2 (D_1 + D_2)^2 (4D_1 + 2D_2)} \right] + \text{h.o.t.} , \quad (\text{S-6})$$

shown in Fig. 3. In the validity regime, the leading order of the entropy production in (S-6) is nonnegative, as can be seen by using the Cauchy-Schwarz inequality  $a_1^2/D_1 + a_2^2/D_2 \geq (a_1 + a_2)^2/(D_1 + D_2)$ . In fact, the first term in the right-hand side of Eq. (S-6) vanishes if  $a_1/D_1 = a_2/D_2$ , which is, precisely, the detailed balance condition for this case, Eq. (5). However, outside of this validity regime, Eq. (S-6) clearly provides an unphysical result, as the entropy production rate is predicted to be negative. The remedy to this unphysical result lies in the higher order corrections in the perturbation expansion.

## DOI-PELITI FIELD THEORY OF AN INTERACTING PARTICLE SYSTEM

The Fokker-Planck equation of the joint probability density  $P(x, \mathbf{y}; t)$  of the system described by Eq. (1) is

$$\partial_t P(x, \mathbf{y}; t) = \left\{ D_1 \partial_x^2 - u_1 \partial_x + \sum_{i=1}^N (D_2 \partial_{y_i}^2 - u_2 \partial_{y_i}) \right\} P(x, \mathbf{y}; t) \quad (\text{S-7a})$$

$$+ \sum_{i=1}^N \left\{ \partial_x (V'_1(x - y_i) P(x, \mathbf{y}; t)) + \partial_{y_i} (V'_2(y_i - x) P(x, \mathbf{y}; t)) \right\}, \quad (\text{S-7b})$$

where  $P(x, \mathbf{y}; t)$  is invariant under permutations of the positions  $y_i$  due to the indistinguishability of B particles.

The Doi-Peliti action of this stochastic process follows from the Fokker-Planck Eq. (S-7) [15, 29, 30]. We introduce the annihilation field  $\phi(x, t)$  and the Doi-shifted creation field  $\tilde{\phi}(x, t)$  for species A and, similarly,  $\psi(y, t)$  and  $\tilde{\psi}(y, t)$  for species B. Even though there may be multiple particles of each species, the action functional  $\mathcal{A}[\phi, \tilde{\phi}, \psi, \tilde{\psi}]$  is derived from the single particle dynamics [15]. In this paper, we use the convention that an observable  $\bullet$  is calculated via the path integral  $\langle \bullet \rangle = \int \mathcal{D}[\phi, \tilde{\phi}, \psi, \tilde{\psi}] \bullet \exp(\mathcal{A}[\phi, \tilde{\phi}, \psi, \tilde{\psi}])$ . We split the action into two parts,  $\mathcal{A} = \mathcal{A}_0 + \mathcal{A}_{\text{pert}}$ , where  $\mathcal{A}_0$ , derived from (S-7a), governs free motion of particles,

$$\mathcal{A}_0 = \int dt \int_0^L dx \tilde{\phi} \left\{ -\partial_t + D_1 \partial_x^2 - u_1 \partial_x \right\} \phi + \int dt \int_0^L dy \tilde{\psi} \left\{ -\partial_t + D_2 \partial_y^2 - u_2 \partial_y \right\} \psi, \quad (\text{S-8})$$

and  $\mathcal{A}_{\text{pert}}$ , derived from (S-7b), governs particle interactions [31]

$$\mathcal{A}_{\text{pert}} = - \int dt \int_0^L dx \int_0^L dy \left\{ (\partial_x \tilde{\phi}) \phi [\partial_x V_1(x - y)] (\tilde{\psi} + 1) \psi + (\partial_y \tilde{\psi}) \psi [\partial_y V_2(y - x)] (\tilde{\phi} + 1) \phi \right\}. \quad (\text{S-9})$$

To derive  $\mathcal{A}_0$ , we have used that the number of particles is conserved and, therefore,  $\int dx \tilde{\phi}(x, t) \phi(x, t) = 1$  and  $\int dy \tilde{\psi}(y, t) \psi(y, t) = 1$ . To derive the first term in  $\mathcal{A}_{\text{pert}}$  we have used that the effect of interactions on A particles at  $x$  due to the presence of B particles at  $y$  is proportional to the number of B particles  $y$ , which is measured by the number operator  $\psi^\dagger \psi = (\psi + 1) \psi$ , where  $\psi^\dagger = (\psi + 1)$  is the creator field. The second term in  $\mathcal{A}_{\text{pert}}$  is derived similarly. To calculate an observable  $\bullet$ , we do so order by order, in the perturbation expansion  $\langle \bullet \rangle = \langle \bullet \exp(\mathcal{A}_{\text{pert}}) \rangle_0 = \langle \bullet (1 + \mathcal{A}_{\text{pert}} + \dots) \rangle_0$  about the Gaussian model given by  $\mathcal{A}_0$  assuming weak interactions.

We express the fields in Fourier space following the convention

$$\overset{(\sim)}{\phi}(x, t) = \frac{1}{L} \sum_n \int d\omega e^{-i\omega t + ik_n x} \overset{(\sim)}{\phi}_n(\omega) \quad \text{and} \quad \overset{(\sim)}{\phi}_n(\omega) = \int_0^L dy \int dt e^{i\omega t - ik_n x} \overset{(\sim)}{\phi}(x, t), \quad (\text{S-10})$$

where  $d = d/(2\pi)$  and  $k_n = 2\pi n/L$ , and similarly for  $\overset{(\sim)}{\psi}$ , as well as the interaction potentials,

$$V_1(x - y) = \frac{1}{L} \sum_n e^{ik_n(x-y)} \mu_n, \quad (\text{S-11a})$$

$$V_2(x - y) = \frac{1}{L} \sum_n e^{ik_n(x-y)} \nu_n. \quad (\text{S-11b})$$

The Gaussian part of the action in Eq. (S-8) in Fourier space reads

$$\begin{aligned} \mathcal{A}_0 \left[ \phi_n(\omega), \tilde{\phi}_{n'}(\omega'), \psi_n(\omega), \tilde{\psi}_{n'}(\omega') \right] &= \int d\omega d\omega' \delta(\omega + \omega') \frac{1}{L^2} \sum_{n, n'=-\infty}^{\infty} L \delta_{n, n'} \\ &\times \left\{ \tilde{\phi}_{n'}(\omega') (-i\omega + D_1 k_n^2 - iu_1 k_n) \phi_n(\omega) + \tilde{\psi}_{n'}(\omega') (-i\omega + D_2 k_n^2 - iu_2 k_n) \psi_n(\omega) \right\}, \end{aligned} \quad (\text{S-12})$$

and the part governing interactions in Eq. (S-9) is,

$$\mathcal{A}_{\text{pert}} \left[ \phi_n(\omega_1), \tilde{\phi}_{n'}(\omega'_1), \psi_n(\omega_2), \tilde{\psi}_{n'}(\omega'_2) \right] \quad (\text{S-13})$$

$$\begin{aligned}
&= \int d\omega_1 d\omega'_1 d\omega_2 d\omega'_2 \delta(\omega_1 + \omega'_1 + \omega_2 + \omega'_2) \frac{1}{L^4} \sum_{n,n',m,m'} L\delta_{n+n'+m+m',0} \\
&\quad \times (\mu_{-n-n'} k_{n'} k_{-n-n'} + \nu_{-m-m'} k_{m'} k_{-m-m'}) \tilde{\phi}_{n'}(\omega'_1) \phi_n(\omega_1) \tilde{\psi}_{m'}(\omega'_2) \psi_m(\omega_2) \\
&+ \int d\omega_1 d\omega'_1 d\omega_2 \delta(\omega_1 + \omega'_1 + \omega_2) \frac{1}{L^3} \sum_{n,n',m} L\delta_{n+n'+m,0} \mu_{-n-n'} k_{n'} k_{-n-n'} \tilde{\phi}_{n'}(\omega'_1) \phi_n(\omega_1) \psi_m(\omega_2) \\
&+ \int d\omega_1 d\omega_2 d\omega'_2 \delta(\omega_1 + \omega_2 + \omega'_2) \frac{1}{L^3} \sum_{n,m,m'} L\delta_{n+m+m',0} \nu_{-m-m'} k_{m'} k_{-m-m'} \phi_n(\omega_1) \tilde{\psi}_{m'}(\omega'_2) \psi_m(\omega_2) . \quad (\text{S-14})
\end{aligned}$$

The bare propagators in Fourier space read, from Eq. (S-12),

$$n, \underline{\omega} \quad n', \omega' \hat{=} \left\langle \phi_n(\omega) \tilde{\phi}_{n'}(\omega') \right\rangle_0 = \frac{L \delta_{n+n',0} \delta(\omega + \omega')}{-i\omega + D_1 k_n^2 + iu_1 k_n + r} , \quad (\text{S-15a})$$

$$\overset{n, \omega}{\sim\!\!\!\sim\!\!\!\sim} \overset{n', \omega'}{\sim\!\!\!\sim\!\!\!\sim} \hat{=} \left\langle \psi_n(\omega) \tilde{\psi}_{n'}(\omega') \right\rangle_0 = \frac{L \delta_{n+n', 0} \delta(\omega + \omega')}{-i\omega + D_2 k_n^2 + iu_2 k_n + r} , \quad (\text{S-15b})$$

where  $r$  is the mass,  $\delta = 2\pi\delta$  is the Dirac  $\delta$  function and  $\delta_{n,m}$  is the Kronecker  $\delta$  function. The mass  $r$  is to be taken to zero after inverting the Fourier transform. In Eq. (S-15), the diagrams  and  represent the bare propagators of species A and B respectively, where time is read from right to left. The nonlinear couplings in  $\mathcal{A}_{\text{pert}}$  involve a four-point vertex and three-point vertices,

$$\begin{array}{c} n' \quad n \\ \hline \text{---} \\ m' \quad m \end{array} \hat{=} \frac{1}{L^3} (\mu_{-n-n'} k_{n'} k_{-n-n'} + \nu_{-m-m'} k_{m'} k_{-m-m'}) \delta_{n+n'+m+m',0} \delta(\omega_1 + \omega'_1 + \omega_2 + \omega'_2) , \quad (\text{S-16a})$$

$$\overbrace{\overbrace{\overbrace{n}^n}^n}^n \hat{=} \frac{1}{L^2} \mu_{-n-n'} k_{n'} k_{-n-n'} \delta_{n+n'+m,0} \delta(\omega_1 + \omega'_1 + \omega_2) , \quad (\text{S-16b})$$

$$\overbrace{m' \quad \quad \quad m}^n \hat{=} \frac{1}{L^2} \nu_{-m-m'} k_{m'} k_{-m-m'} \delta_{n+m+m',0} \delta(\omega_1 + \omega_2 + \omega'_2) . \quad (S-16c)$$

The dashed line  $\text{---}$  represents an interaction between two particles mediated by a potential. Diagrammatically, a potential has a similar representation as a propagator, with the difference that it is represented vertically, since the potential has no time dependence because its effect is *propagated* instantly.

## TWO-POINT CORRELATION FUNCTION

## Two-particle system

The stationary correlation function  $P_2^{(2)}(x, y) = \lim_{t \rightarrow \infty} \langle \phi(x, t)\psi(y, t)\phi^\dagger(x_0, t_0)\psi^\dagger(y_0, t_0) \rangle$  gives the probability that particles A and B are found at positions  $x$  and  $y$ , respectively, in the limit  $t \rightarrow \infty$ . Since the system is finite and the dynamics are conservative, the existence of the stationary limit is guaranteed. Doi-shifting the creation fields in the observable,  $\phi^\dagger = 1 + \tilde{\phi}$  and  $\psi^\dagger = 1 + \tilde{\psi}$ , produces  $\langle \phi\psi\phi^\dagger\psi^\dagger \rangle = \langle \phi\psi\tilde{\phi}\tilde{\psi} \rangle + \langle \phi\psi \rangle + \langle \phi\psi\tilde{\phi} \rangle + \langle \phi\psi\tilde{\psi} \rangle$ , where the last three terms are all zero because there is no matching vertex in  $\mathcal{A}_{\text{pert}}$ .

## The stationary correlation function

$$P_2^{(2)}(x, y) = \lim_{t \rightarrow \infty} \left\langle \phi(x, t) \psi(y, t) \tilde{\phi}(x_0, t_0) \tilde{\psi}(y_0, t_0) \right\rangle \hat{=} \quad \text{Diagram: } \begin{array}{c} x \\ \hline y \end{array} + \quad \text{Diagram: } \begin{array}{c} x \\ \hline y \end{array} + \quad \text{Diagram: } \begin{array}{c} x \\ \hline y \end{array} + \quad \text{Diagram: } \begin{array}{c} x \\ \hline y \end{array} + \dots \quad (\text{S-17})$$

is independent of the initial conditions  $x_0, y_0$  since the only contributing Fourier modes in the limit  $t \rightarrow \infty$  are the zeroth modes  $\tilde{\phi}_0$  and  $\tilde{\psi}_0$  [22, 32]. This is reflected in the diagrams by their amputated incoming legs. We expand the Fourier space representation of the two-point correlation

$$P_2^{(2)}(x, y) = \frac{1}{L^4} \sum_{n=-\infty}^{\infty} e^{ik_n(x-y)} \langle \phi_n \psi_{-n} \tilde{\phi}_0 \tilde{\psi}_0 \rangle , \quad (\text{S-18})$$

perturbatively in small  $\mu$  and  $\nu$  compared to the diffusion constants  $D_1$  and  $D_2$ ,

$$\langle \phi_n \psi_{-n} \tilde{\phi}_0 \tilde{\psi}_0 \rangle = \sum_{j=0}^{\infty} \frac{1}{j!} \langle \phi_n \psi_{-n} \tilde{\phi}_0 \tilde{\psi}_0 (\mathcal{A}_{\text{pert}})^j \rangle_0 = \sum_{j=0}^{\infty} G_j(n) . \quad (\text{S-19})$$

The  $j$ -th order in the perturbation expansion of the  $n$ -th Fourier mode of  $P_2^{(2)}$  is, diagrammatically,

$$G_j(n) \hat{=} \begin{array}{c} j \\ \overbrace{\quad \quad \quad \quad \quad} \\ n \quad \dots \quad 0 \\ \hline -n \quad \dots \quad 0 \end{array} , \quad (\text{S-20})$$

where the incoming legs carry the zeroth Fourier mode only. The  $j$ -th order correction  $G_j$  is made of  $j$  four-legged interaction vertices attached to  $j$  propagators of each species forming a chain of  $j-1$  loops. The  $(j+1)$ -th order  $G_{j+1}$  is generated from  $G_j$  by attaching an interaction vertex (S-16a) to the outgoing legs, effectively creating a new loop,

$$\begin{aligned} G_{j+1}(n) &\hat{=} \sum_m \int d\omega \begin{array}{c} j+1 \\ \overbrace{\quad \quad \quad \quad \quad} \\ n, \omega \quad -n \quad m \quad \dots \quad 0 \\ \hline -n, -\omega \quad n \quad -m \quad \dots \quad 0 \end{array} \\ &\hat{=} \frac{1}{L} \sum_m \int d\omega I_n \frac{\mu_{n-m} k_{-n} k_{n-m} + \nu_{-n+m} k_n k_{-n+m}}{(-i\omega + D_1 k_n^2 + iu_1 k_n)(i\omega + D_2 k_n^2 - iu_2 k_n)} G_j(m) \\ &= \frac{I_n}{L} \sum_m \frac{(\mu_{n-m} + \nu_{-n+m}) k_{-n+m}}{(D_1 + D_2) k_n + i(u_1 - u_2)} G_j(m) , \end{aligned} \quad (\text{S-21})$$

where  $I_n = 1 - \delta_{n,0}$  ensures that  $G_j(0) = 0$  for  $j > 0$ . The zeroth-order term is, trivially, the constant zeroth Fourier mode  $G_0(n) = L^2 \delta_{n,0}$ .

The iterative scheme in Eq. (S-21) has the same structure as the recurrence relation found in the stationary probability distribution of a drift-diffusive particle in a periodic potential [28]. Therefore, by mapping the two systems, the two-point correlation function follows straight-forwardly,  $P_2^{(2)}(x, y) = \rho(x - y)/L$ , with

$$\rho(\ell) = \frac{1}{L\mathcal{N}} e^{-\frac{V_1(\ell) + V_2(-\ell) - (u_1 - u_2)\ell}{D_1 + D_2}} \int_{\ell}^{\ell+L} d\ell' e^{\frac{V_1(\ell') + V_2(-\ell') - (u_1 - u_2)\ell'}{D_1 + D_2}} , \quad (\text{S-22})$$

where the constant  $\mathcal{N}$  is such that  $\int_0^L d\ell \rho(\ell) = 1$  [27, Eq. (11.37)], shown in Fig. 2. Although our argument is based on a perturbation expansion about small couplings  $\nu$  and  $\mu$ , the exact result in Eq. (S-22) is valid for any couplings because the map between  $G_{j+1}$  in Eq. (S-21) and the analogous  $G_{j+1}$  in [28] holds for all orders  $j \in \{0, 1, \dots\}$ .

### Many-particle system

In the many-particle system, the two-point correlation function  $P_2^{(1+N)}(x, y)$  is the probability of finding the only particle of species A at position  $x$ , and one out of  $N$  particles of species B at  $y$ . This observable is represented as the following path integral and diagrammatic perturbation expansion,

$$P_2^{(1+N)}(x, y) = \lim_{t \rightarrow \infty} N \langle \phi(x, t) \psi(y, t) \phi^\dagger(x_0, t_0) \psi^\dagger(y_1, t_0) \psi^\dagger(y_2, t_0) \dots \psi^\dagger(y_N, t_0) \rangle$$

$$\begin{aligned}
&\stackrel{\hat{=}}{=} \lim_{t \rightarrow \infty} N \left( \begin{array}{c} x \text{---} \\ y \text{---} \end{array} + \dots \right. \\
&\quad \left. + (N-1) \left( \begin{array}{c} x \text{---} \\ y \text{---} \end{array} + \begin{array}{c} x \text{---} \\ y \text{---} \end{array} + \begin{array}{c} x \text{---} \\ y \text{---} \end{array} + \dots \right) + \dots \right), \quad (\text{S-23})
\end{aligned}$$

up to third order in the interaction vertices. In principle, there are more terms that enter in this observable than those shown in Eq. (S-23). However, terms such as

$$\lim_{t \rightarrow \infty} \begin{array}{c} x \text{---} \\ y \text{---} \end{array} = \lim_{t \rightarrow \infty} \begin{array}{c} x \text{---} \\ y \text{---} \end{array} = \lim_{t \rightarrow \infty} \begin{array}{c} x \text{---} \\ y \text{---} \end{array} \stackrel{\hat{=}}{=} 0 \quad (\text{S-24})$$

do not contribute in the limit  $t \rightarrow \infty$  because of factors  $k_0$  in the interaction vertices in Eq. (S-16).

The sinusoidal interaction potentials  $V_1(\ell) = a_1 \cos k_1 \ell$  and  $V_2(\ell) = a_2 \cos k_1 \ell$  only have two nonzero Fourier modes,

$$\mu_1 = \mu_{-1} = \frac{a_1 L}{2}, \quad \nu_1 = \nu_{-1} = \frac{a_2 L}{2}, \quad (\text{S-25})$$

and  $\mu_n = \nu_n = 0$  for  $n \neq \pm 1$ , and we further assume zero drift  $u_1 = u_2 = 0$ . The terms in Eq. (S-23) involving the only A particle and one of the B particles are, therefore,

$$\lim_{t \rightarrow \infty} \begin{array}{c} x \text{---} \\ y \text{---} \end{array} \stackrel{\hat{=}}{=} \frac{1}{L^4} \sum_n e^{ik_n(x-y)} G_0(n) = \frac{1}{L^2} \quad (\text{S-26a})$$

$$\lim_{t \rightarrow \infty} \begin{array}{c} x \text{---} \\ y \text{---} \end{array} \stackrel{\hat{=}}{=} \frac{1}{L^4} \sum_n e^{ik_n(x-y)} G_1(n) = -\frac{1}{L^2} \frac{a_1 + a_2}{D_1 + D_2} \cos k_1(x-y) \quad (\text{S-26b})$$

$$\lim_{t \rightarrow \infty} \begin{array}{c} x \text{---} \\ y \text{---} \end{array} \stackrel{\hat{=}}{=} \frac{1}{L^4} \sum_n e^{ik_n(x-y)} G_2(n) = \frac{1}{L^2} \left( \frac{a_1 + a_2}{D_1 + D_2} \right)^2 \frac{\cos k_2(x-y)}{4} \quad (\text{S-26c})$$

$$\lim_{t \rightarrow \infty} \begin{array}{c} x \text{---} \\ y \text{---} \end{array} \stackrel{\hat{=}}{=} \frac{1}{L^4} \sum_n e^{ik_n(x-y)} G_3(n) = \frac{1}{L^2} \left( \frac{a_1 + a_2}{D_1 + D_2} \right)^3 \left( \frac{\cos k_1(x-y)}{8} - \frac{\cos k_3(x-y)}{24} \right), \quad (\text{S-26d})$$

where  $G_j(n)$  is defined in Eq. (S-20). The terms in Eq. (S-23) involving two B particles are,

$$\begin{aligned}
&\lim_{t \rightarrow \infty} \begin{array}{c} x \text{---} \\ y \text{---} \end{array} \stackrel{\hat{=}}{=} \frac{1}{L^5} \sum_{n,i} e^{ik_n(x-y)} \int d\omega d\omega' \\
&\quad \frac{(\mu_n k_{-n} k_n + \nu_{-n} k_n k_{-n}) \mu_{-i} k_{-n} k_{-i} (\mu_i k_{-n-i} k_i + \nu_{-i} k_i k_{-i})}{(-i\omega + D_1 k_n^2 + r)(-i\omega + D_1 k_n^2 + r)(i\omega + D_2 k_n^2 + r)(-i(\omega + \omega') + D_1 k_{n+i}^2 + r)(i\omega' + D_2 k_i^2 + r)} \\
&\quad = \frac{1}{L^2} \frac{a_1(a_1 + a_2)(a_1 D_2 - a_2 D_1)}{4D_2(D_1 + D_2)^2(2D_1 + D_2)} \cos k_1(x-y) \quad (\text{S-27a})
\end{aligned}$$

$$\lim_{t \rightarrow \infty} \begin{array}{c} x \text{---} \\ y \text{---} \end{array} \stackrel{\hat{=}}{=} \frac{1}{L^5} \sum_{n,i} e^{ik_n(x-y)} \int d\omega d\omega' \quad (\text{S-27b})$$

$$\begin{aligned}
& \frac{(\mu_i k_{-i} k_i + \nu_{-i} k_i k_{-i}) \mu_{-i} k_{-n} k_{-i} (\mu_n k_{-n-i} k_n + \nu_{-n} k_n k_{-n})}{(-i\omega + D_1 k_n^2 + r)(-i(\omega + \omega') + D_1 k_{n+i}^2 + r)(-i\omega' + D_1 k_i^2 + r)(i\omega + D_2 k_n^2 + r)} \\
& = \frac{1}{L^2} \frac{a_1(a_1 + a_2)(a_1 D_2 - a_2 D_1)}{4D_2(D_1 + D_2)^2(2D_1 + D_2)} \cos k_1(x - y) . \tag{S-27b}
\end{aligned}$$

Using Eqs. (S-26) and (S-27) in Eq. (S-23), we obtain the two-point correlation function perturbatively up to third order,

$$\begin{aligned}
P_2^{(1+N)}(x, y) &= \frac{N}{L^2} \left[ 1 - \frac{a_1 + a_2}{D_1 + D_2} \cos k_1(x - y) + \frac{1}{4} \left( \frac{a_1 + a_2}{D_1 + D_2} \right)^2 \cos k_2(x - y) \right. \\
&\quad + \frac{1}{24} \left( \frac{a_1 + a_2}{D_1 + D_2} \right)^3 (3 \cos k_1(x - y) - \cos k_3(x - y)) \\
&\quad \left. + (N-1) \frac{a_1(a_1 + a_2)(a_1 D_2 - a_2 D_1)}{2D_2(D_1 + D_2)^2(2D_1 + D_2)} \cos k_1(x - y) \right] + \text{h.o.t.} . \tag{S-28}
\end{aligned}$$

### THREE-POINT CORRELATION FUNCTION

The three-point correlation function of the position  $x$  of the A particle and positions  $y$  and  $y'$  of two B particles in the stationary state is

$$\begin{aligned}
P_3^{(1+N)}(x, y, y') &= \lim_{t \rightarrow \infty} N(N-1) \langle \phi(x, t) \psi(y, t) \psi(y', t) \phi^\dagger(x_0, t_0) \psi^\dagger(y_1, t_0) \psi^\dagger(y_2, t_0) \dots \psi^\dagger(y_N, t_0) \rangle \\
&\stackrel{\hat{=}}{=} \lim_{t \rightarrow \infty} N(N-1) \left( \begin{array}{c} \text{Diagram 1} \quad \text{Diagram 2} \quad \text{Diagram 3} \quad \text{Diagram 4} \quad \text{Diagram 5} \quad \text{Diagram 6} \quad \text{Diagram 7} \quad \dots \\ \text{Diagram 8} \quad \text{Diagram 9} \quad \text{Diagram 10} \quad \text{Diagram 11} \quad \text{Diagram 12} \quad \text{Diagram 13} \quad \text{Diagram 14} \end{array} \right) . \tag{S-29}
\end{aligned}$$

We assume sinusoidal interaction potentials  $V_1(\ell) = a_1 \cos k_1 \ell$  and  $V_2(\ell) = a_2 \cos k_1 \ell$ , and zero drifts  $u_1 = u_2 = 0$ . We distinguish two types of terms in Eq. (S-29): those where a propagator  is decoupled from the other two propagators, and those where all three propagators are coupled through interaction vertices. In the first case, the corresponding diagrams can be calculated straightforwardly using the results in (S-26) multiplying by  $1/L$ . For example,

$$\begin{aligned}
\text{Diagram 1} &= \frac{1}{L} \frac{x}{y} = -\frac{1}{L^3} \frac{a_1 + a_2}{D_1 + D_2} \cos k_1(x - y) . \tag{S-30}
\end{aligned}$$

Then, we only need to evaluate the last two diagrams in (S-29), which are symmetric under swapping  $y$  and  $y'$ ,

$$\begin{aligned}
\lim_{t \rightarrow \infty} \text{Diagram 14} &\stackrel{\hat{=}}{=} \frac{1}{L^5} \sum_{n,m} e^{ik_n(x-y)+ik_m(x-y')} \int d\omega d\omega' \\
&\quad \frac{(\mu_m k_{-n-m} k_m + \nu_{-m} k_m k_{-m})(\mu_n k_{-n} k_n + \nu_{-n} k_n k_{-n})}{(-i(\omega + \omega') + D_1 k_{n+m}^2 + r)(-i\omega + D_1 k_n^2 + r)(i\omega + D_2 k_n^2 + r)(i\omega' + D_2 k_m^2 + r)} \\
&= \frac{1}{2L^3} \frac{a_1 + a_2}{D_1 + D_2} \left\{ \frac{a_2}{2D_2} \cos k_1(y - y') + \frac{a_2 + 2a_1}{4D_1 + 2D_2} \cos k_1(2x - y - y') \right\} . \tag{S-31}
\end{aligned}$$

In fact, Eq. (S-31) is invariant under exchange of  $y$  and  $y'$ , so the two last terms in the right-hand side of (S-29) are therefore equal. We obtain the three-point correlation function up to second order in the perturbation expansion by

using Eqs. (S-26) and (S-31), in Eq. (S-29),

$$\begin{aligned} P_3^{(1+N)}(x, y, y') = & \frac{N(N-1)}{L^3} \left[ 1 - \frac{a_1 + a_2}{D_1 + D_2} (\cos k_1(x-y) + \cos k_1(x-y')) \right. \\ & + \frac{1}{4} \left( \frac{a_1 + a_2}{D_1 + D_2} \right)^2 (\cos k_2(x-y) + \cos k_2(x-y')) \\ & \left. + \frac{a_1 + a_2}{2(D_1 + D_2)} \left\{ \frac{a_2}{D_2} \cos k_1(y-y') + \frac{2a_1 + a_2}{2D_1 + D_2} \cos k_1(2x-y-y') \right\} \right] + \text{h.o.t. .} \end{aligned} \quad (\text{S-32})$$

The correlation functions in Eqs. (S-28) and (S-32) can also be obtained by performing a Taylor expansion about the equilibrium distribution in Eq. (7), with  $a_1/D_1 = a_2/D_2$ , where the normalisation constant also needs to be expanded.

Marginalising Eq. (S-32), we obtain the two-point correlation function between two particles of species B at positions  $y$  and  $y'$ ,

$$P_{B,B}^{(1+N)}(y, y') = \int_0^L dx P_3^{(1+N)}(x, y, y') = \frac{N(N-1)}{L^2} \left[ 1 + \frac{a_2(a_1 + a_2)}{2D_2(D_1 + D_2)} \cos k_1(y-y') \right] + \text{h.o.t. ,} \quad (\text{S-33})$$

whose second-order correction indicates the effective interactions between particles of species B, shown in Fig. 4.